

This is a pre print version of the following article:

Effect Of Pair Coalescence Of Circular Pores On The Overall Elastic Properties / Lanzoni, L.; Radi, E.; Sevostianov, I.. - In: INTERNATIONAL JOURNAL OF SOLIDS AND STRUCTURES. - ISSN 0020-7683. - 172:(2019), pp. 38-50. [10.1016/j.ijsolstr.2019.05.012]

Terms of use:

The terms and conditions for the reuse of this version of the manuscript are specified in the publishing policy. For all terms of use and more information see the publisher's website.

06/05/2026 10:33

(Article begins on next page)

Dear author,

Please note that changes made in the online proofing system will be added to the article before publication but are not reflected in this PDF.

We also ask that this file not be used for submitting corrections.



Contents lists available at ScienceDirect

International Journal of Solids and Structures

journal homepage: www.elsevier.com/locate/ijsolstr

Effect of pair coalescence of circular pores on the overall elastic properties

L. Lanzoni^a, E. Radi^b, I. Sevostianov^{c,*}^a Dipartimento di Ingegneria "Enzo Ferrari", Università di Modena e Reggio Emilia, Via Vivarelli, 10 41125 Modena, Italy^b Dipartimento di Scienze e Metodi dell'Ingegneria, Università di Modena e Reggio Emilia, Via Amendola, 2 42122 Reggio Emilia, Italy^c Department of Mechanical and Aerospace Engineering, New Mexico State University, Las Cruces, NM 88001, USA

ARTICLE INFO

Article history:

Received 28 February 2019

Revised 14 May 2019

Accepted 14 May 2019

Available online xxx

Keywords:

Cylindrical pores

Irregular cross-section

Bipolar coordinates

Compliance contribution tensor

Effective elastic

ABSTRACT

The paper focuses on the effect of the pair coalescence of circular pores on the overall elastic properties. An analytic solution for the stress and displacement fields in an infinite elastic medium, containing cylindrical pore with the cross-section formed by two circles, and subjected to remotely applied uniform stresses is obtained. The displacement field on the surface of the pore is then determined as a function of the geometrical parameters. This result is used to calculate compliance contribution tensor for the pore and to evaluate effective elastic properties of a material containing multiple pores of such a shape.

© 2019 Elsevier Ltd. All rights reserved.

1. Introduction

In the present paper we focus on the effect of the pair coalescence of circular pores on the overall elastic properties. The research is motivated mostly by the needs to predict properties of porous materials obtained by Gasar technology – process consisting of a melting metal in a gas atmosphere to saturate it with hydrogen and directional solidification (Shapovalov, 1994; Shapovalov and Boyko, 2004). The pores have cylindrical shape and are nucleated heterogeneously. The process is accompanied by pores coalescence. Shapovalov (1998) showed that the pore coalescence becomes prominent for Gasar metals with high porosity. The modeling of the evolution process of pore coalescence has been proposed by Liu et al. (2018). Fig. 1 illustrates the process of the pores coalescence and the resulting shapes of the pores' cross-sections in Gasar metals.

We consider this material in the framework of plane-strain problem and assume that it contains aligned cylindrical inhomogeneities of certain cross-sectional shape. Analytical modeling of materials with inhomogeneities of non-elliptical cross-section is not well developed though many two-dimensional problems have been solved. The main approaches to this problem are:

- Complex variables technique involving conformal mapping of the cross-sectional shape onto a unit circle (Kachanov et al., 1994). For many non-elliptical shapes, the transformation

$$z(\zeta) = R \left(\frac{1}{\zeta} + \sum_{n=1}^N a_n \zeta^n \right) \quad (1.1)$$

that maps conformally the exterior of the inhomogeneity in the complex z -plane into the interior of a unit circle in the ζ -plane, is used, with parameters R , N and a_n corresponding to various shapes; for the elliptical hole, for example, $N=1$, $R=(a+b)/2$ and $a_1=(a-b)/(a+b)$. For "irregular" shapes, a numerical mapping technique can be used (see Tsukrov and Novak, 2004);

- Finite element method, that is more universal, applies to inhomogeneities of arbitrary elastic properties, including anisotropic ones, but has lower accuracy than the numerical conformal mapping technique. Comparison of the two methods was given by Tsukrov and Novak (2002).

Compressibility of non-elliptical holes has been first analyzed by Zimmerman (1986) on the example of super-circular holes (convex and concave), by Givoli and Elishakoff (1992) and Ekneligoda and Zimmerman (2008a) who considered holes with "corrugated" boundaries and by Ekneligoda and Zimmerman (2006, 2008b) who considered shapes having n -fold symmetry axes. Results for the entire compliance contribution tensor of a non-elliptical hole have been obtained by

* Corresponding author.

E-mail address: igor@nmsu.edu (I. Sevostianov).

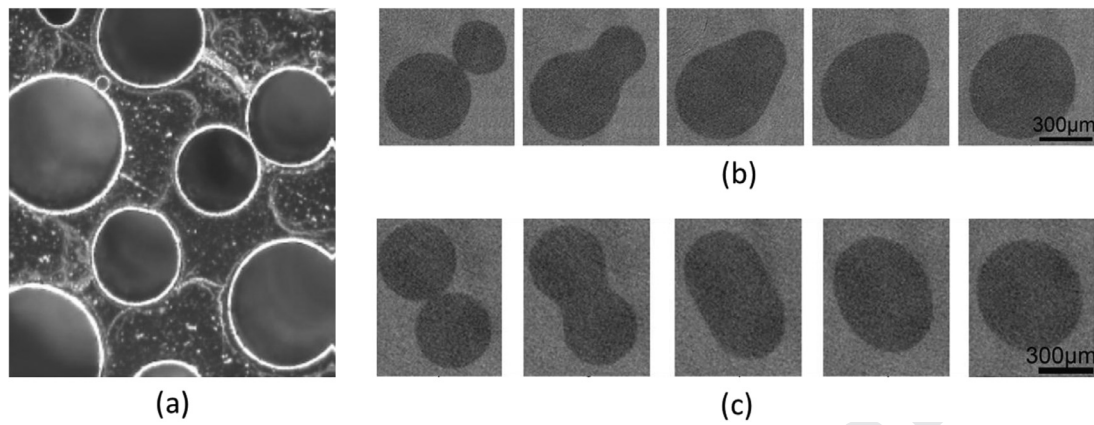


Fig. 1. (a) Pores structure in Gasar Ni-15%Al, intermetallic compound (shape of pores is almost cylindrical, from Drenchev and Sobczak, 2009); (b) and (c) evolution of two pores coalescence in Gasar copper (from Liu et al., 2018).

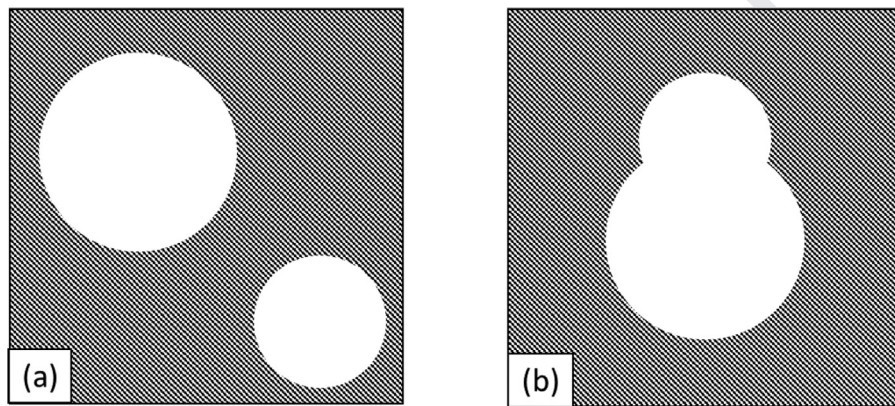


Fig. 2. (a) two separate circular holes, (b) cross-section formed by two coalesced circular pores of generally different radii.

44 Kachanov et al. (1994) and Jasiuk (1995) for various polygons (con-
 45 vex and concave) and Tsukrov and Novak (2002, 2004) for several
 46 “irregular” shapes.

47 The present paper continues authors’ work (Lanzoni et al., 2018)
 48 on the shapes that may be obtained by union of two circles of
 49 generally different diameters (Fig. 2). We consider isotropic elas-
 50 tic plane containing two circular holes of radii r_1 and r_2 (that
 51 may overlap). Thus, the pore shapes may be non-convex and even
 52 not simply connected. Instead of the conformal mapping technique
 53 (that may be a problem in this case since connectivity of the
 54 pore may change) we use an analytic approach based on Fourier
 55 series representation or Fourier transform in bipolar coordinates
 56 (Jeffery, 1921), (α, β) (Fig. 3), related to the Cartesian coordinates
 57 (x_1, x_2) by

$$\alpha = \operatorname{Re} \left[\ln \frac{(x_1 + ix_2) + a}{(x_1 + ix_2) - a} \right]; \quad \beta = -\operatorname{Im} \left[\ln \frac{(x_1 + ix_2) + a}{(x_1 + ix_2) - a} \right]; \quad (1.2)$$

$$x_1 = \frac{a \sinh \alpha}{\cosh \alpha - \cos \beta}; \quad x_2 = \frac{a \sin \beta}{\cosh \alpha - \cos \beta}. \quad (1.3)$$

59 Note, that β -coordinate is multi-valued with a discontinuity of
 60 2π across the segment connecting the foci. Hereinafter, we as-
 61 sume $-\pi < \beta \leq \pi$. The two poles of the bipolar coordinates are
 62 located on the x_1 axis at distance $\pm a$, with $a > 0$ (the circles in
 63 Fig. 2(a) refers to $\alpha_1 > 0$ and $\alpha_2 < 0$ whereas Fig. 2(b) shows two
 64 overlapping circles with $\beta_1 > 0$ and $\beta_2 < 0$).

65 First, we consider a single inhomogeneity and solve Neumann
 66 boundary value problem in two-steps: (1) assessment of the fun-

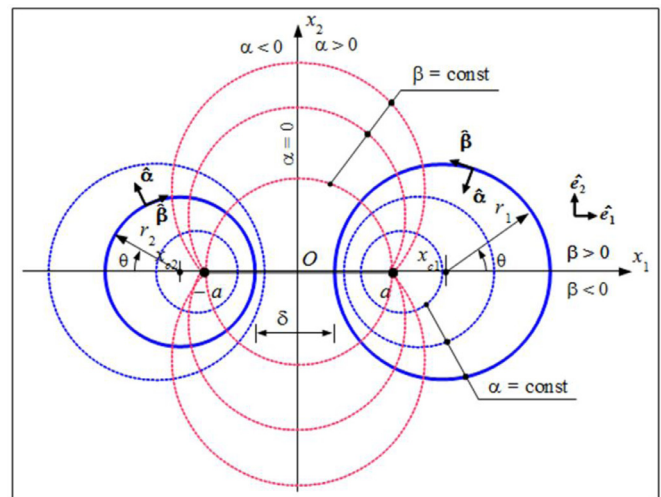


Fig. 3. Sketch of the bipolar coordinate system.

67 damental displacement field related to a remotely applied uniform
 68 stress in a homogeneous body and (2) fulfillment of the boundary
 69 conditions by adding an extra-term to the fundamental field. This
 70 solution is used to construct the compliance contribution tensor of
 71 a pore of interest by calculating proper contour integrals. The compli-
 72 ance contribution tensor can be used to calculate overall elastic
 73 properties of a material containing parallel cylindrical holes with
 74 the cross-sections shown in Fig. 2.

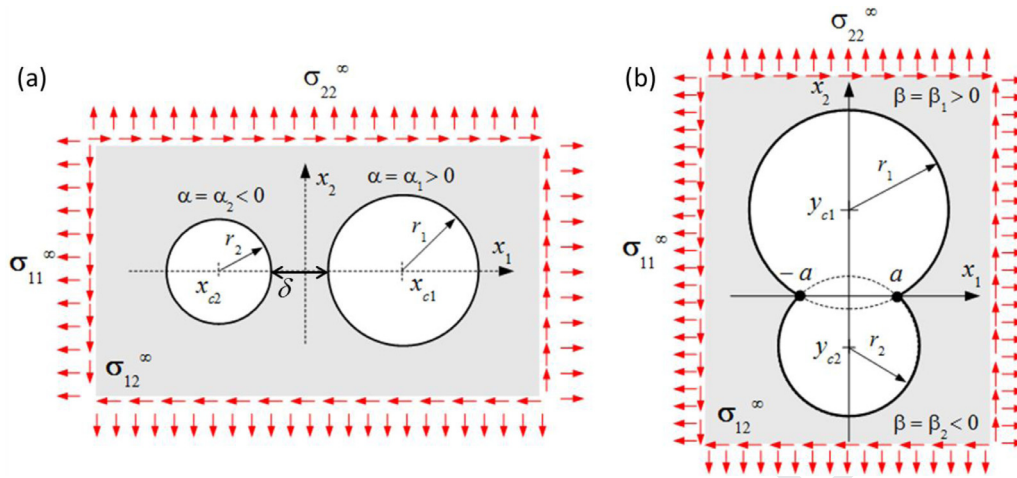


Fig. 4. Sketch of an infinite plate with (a) two separate holes and (b) two merging holes subjected to remote normal σ_{11}^∞ , σ_{22}^∞ and shear σ_{12}^∞ stress fields along the principal directions x_1, x_2 .

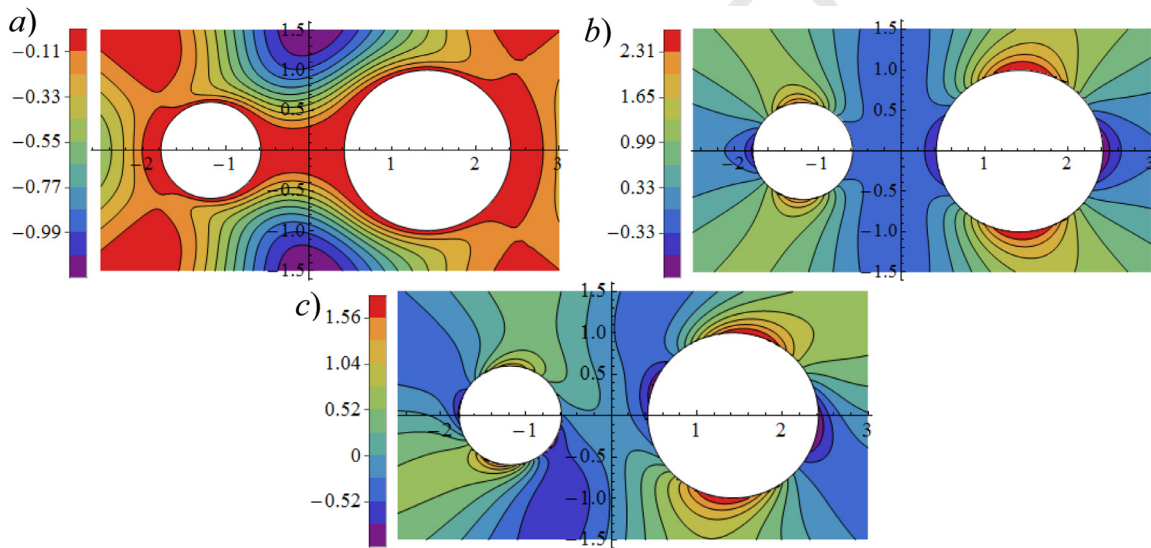


Fig. 5. Distribution of the dimensionless stress fields (a) $\sigma_{\alpha\alpha}/\sigma_{11}^\infty$; (b) $\sigma_{\beta\beta}/\sigma_{11}^\infty$; (c) $\sigma_{\alpha\beta}/\sigma_{11}^\infty$ in a plate subjected to a remote stress in the x_1 direction for $\rho = 3/5$, $\gamma = 1$.

75 **2. Two separate circular holes**

76 In this Section we briefly summarize the known results about
 77 elastic fields in an infinite plate containing two separate circular
 78 holes of radii r_1 and r_2 in an infinite plane separated by the liga-
 79 ment δ between them. For the case of two holes of the same radius
 80 the problem was solved by Ling (1947, 1948a) for remotely applied
 81 normal loadings and by Karunes (1953) for remotely applied shear
 82 loading. Radi (2011) generalized their solutions for two holes of
 83 different radii.

84 The geometry of the problem is completely determined by
 85 two independent geometrical parameters: for example, ratio of the
 86 radii $\rho \equiv r_1/r_2$ and relative length of the ligament $\gamma \equiv \delta/r_1$
 87 (Fig. 4):

$$\begin{aligned} x_{c1} &= r_1 + \delta[1 - (r_1 + 0.5\delta)/(r_1 + r_2 + \delta)]; \\ \alpha_1 &= \operatorname{arccos} h(x_{c1}/r_1); \quad a = r_1 \sinh(\alpha_1); \\ \alpha_2 &= -\operatorname{arcsin} h(a/r_2); \quad x_{c2} = -r_2 \cosh \alpha_2. \end{aligned} \quad (2.1)$$

88 The plane is subjected to the action of remotely applied stresses
 89 σ_{11}^∞ , σ_{22}^∞ , and σ_{12}^∞ .

90 The traction free boundary conditions

$$\sigma_\alpha = \tau_{\alpha\beta} = 0 \text{ for } \alpha = \alpha_1, \alpha_2 \quad (2.2)$$

have to be satisfied at the holes.

The stress field, corresponding to the biharmonic Airy stress
 92 function χ is given by Jeffery (1921):
 93

$$\begin{aligned} \sigma_\alpha &= -\left[(\cosh \alpha - \cos \beta) \frac{\partial^2}{\partial \beta^2} - \sinh \alpha \frac{\partial}{\partial \alpha} - \sin \beta \frac{\partial}{\partial \beta} + \cosh \alpha \right] h_\chi; \\ \sigma_\beta &= -\left[(\cosh \alpha - \cos \beta) \frac{\partial^2}{\partial \alpha^2} - \sinh \alpha \frac{\partial}{\partial \alpha} - \sin \beta \frac{\partial}{\partial \beta} + \cos \beta \right] h_\chi; \\ \tau_{\alpha\beta} &= (\cosh \alpha - \cos \beta) \frac{\partial^2 h_\chi}{\partial \beta \partial \alpha}, \end{aligned} \quad (2.4)$$

where

$$h_\chi = \frac{\chi}{a} (\cosh \alpha - \cos \beta). \quad (2.5)$$

The Airy function χ can be represented as the sum of a funda-
 95 mental stress function $\chi^{(0)}$, which gives the uniform stresses ap-
 96 plied at infinity but does not yield vanishing tractions on the cir-
 97 cular boundaries, and an auxiliary stress function $\chi^{(1)}$, required to
 98 satisfy the boundary conditions (2.2), which gives zero stresses at
 99 infinity. Correspondingly,
 100

$$h_\chi = h_\chi^{(0)} + h_\chi^{(1)}, \quad (2.6)$$

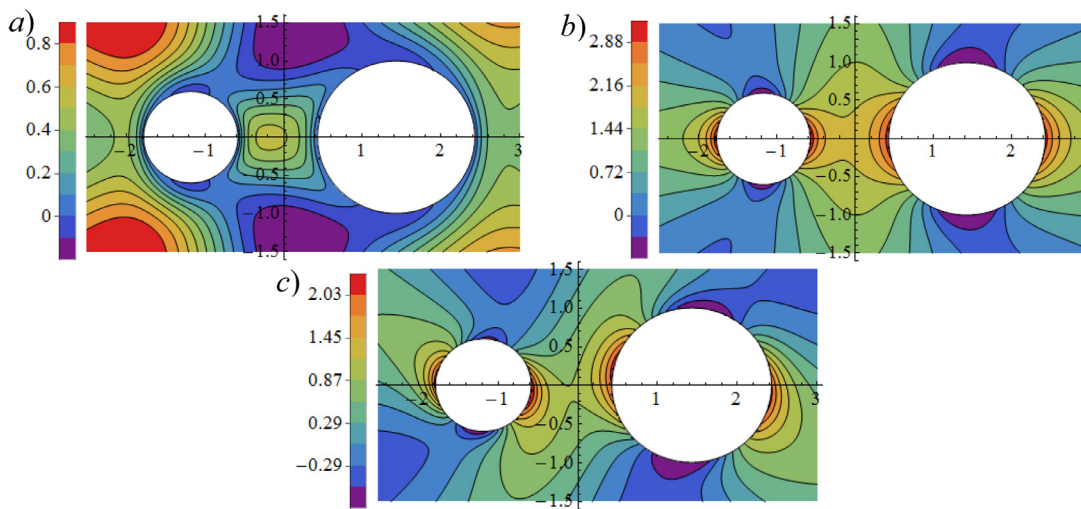


Fig. 6. Distribution of the dimensionless stress fields (a) $\sigma_{\alpha\alpha}/\sigma_{22}^{\infty}$; (b) $\sigma_{\beta\beta}/\sigma_{22}^{\infty}$; (c) $\sigma_{\alpha\beta}/\sigma_{22}^{\infty}$ in a plate subjected to a remote stress in the x_2 direction for $\rho=3/5$, $\gamma=1$.

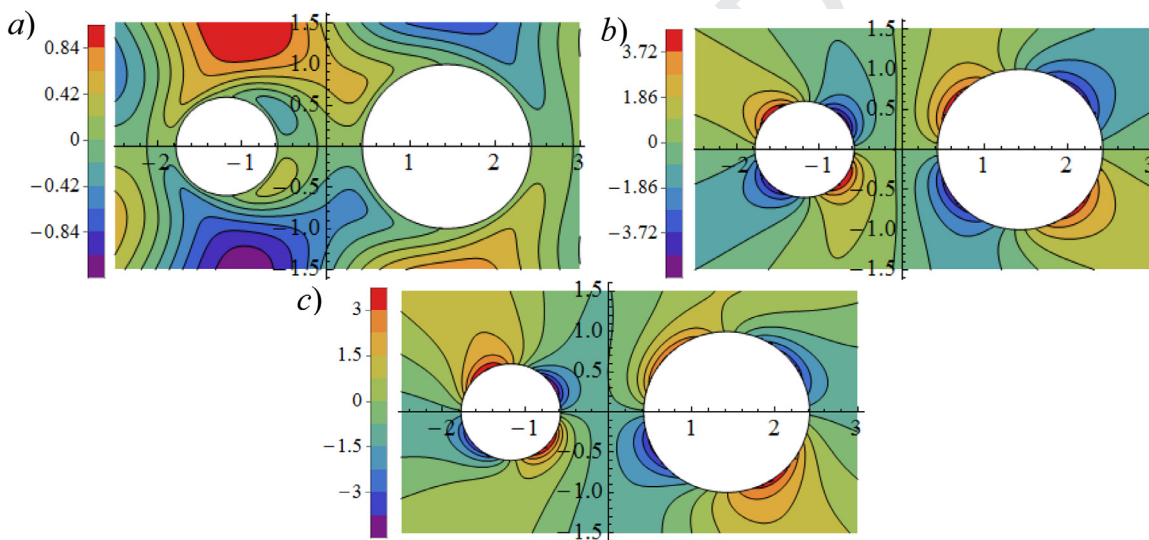


Fig. 7. Distribution of the dimensionless stress fields (a) $\sigma_{\alpha\alpha}/\sigma_{12}^{\infty}$; (b) $\sigma_{\beta\beta}/\sigma_{12}^{\infty}$; (c) $\sigma_{\alpha\beta}/\sigma_{12}^{\infty}$ in a plate subjected to a remote shear stress in the $x_1 \times x_2$ plane for $\rho=3/5$, $\gamma=1$.

101 where

$$h_x^{(0)} = \frac{(\sigma_{11}^{\infty} \sin^2 \beta + \sigma_{22}^{\infty} \sinh^2 \alpha - 2\sigma_{12}^{\infty} \sin \beta \sinh \alpha)}{2(\cosh \alpha - \cos \beta)}. \quad (2.7)$$

$$h_x^{(1)} = [B\alpha + K \ln(\cosh \alpha - \cos \beta)](\cosh \alpha - \cos \beta) + \sum_{n=1}^{\infty} \varphi_n(\alpha) \cos n\beta + \psi_n(\alpha) \sin n\beta. \quad (2.8)$$

103 Functions $\varphi_n(\alpha)$ and $\psi_n(\alpha)$ are given by

$$\begin{aligned} \varphi_n(\alpha) &= A_n \cosh(n+1)\alpha + B_n \cosh(n-1)\alpha \\ &\quad + C_n \sinh(n+1)\alpha + D_n \sinh(n-1)\alpha; \\ \psi_n(\alpha) &= a_n \cosh(n+1)\alpha + b_n \cosh(n-1)\alpha \\ &\quad + c_n \sinh(n+1)\alpha + d_n \sinh(n-1)\alpha, \end{aligned} \quad (2.9)$$

104 The integration constants $B, K, A_n, B_n, C_n, D_n, a_n, b_n, c_n, d_n$ are
105 given in the Appendix A1.

The components of the corresponding displacement vector are
106 given by Jeffery (1921) 107

$$\begin{aligned} 2\mu u_{\alpha} &= (\cosh \alpha - \cos \beta) \left[\frac{\kappa - 1}{2} \frac{\partial}{\partial \alpha} \left(\frac{h_x}{\cosh \alpha - \cos \beta} \right) \right. \\ &\quad \left. - \frac{\kappa + 1}{4} \frac{\partial}{\partial \beta} \left(\frac{h_Q}{\cosh \alpha - \cos \beta} \right) \right], \\ 2\mu u_{\beta} &= (\cosh \alpha - \cos \beta) \left[\frac{\kappa - 1}{2} \frac{\partial}{\partial \beta} \left(\frac{h_x}{\cosh \alpha - \cos \beta} \right) \right. \\ &\quad \left. + \frac{\kappa + 1}{4} \frac{\partial}{\partial \alpha} \left(\frac{h_Q}{\cosh \alpha - \cos \beta} \right) \right], \end{aligned} \quad (2.10)$$

where $\kappa = 3 - 4\nu$ or $\kappa = (3 - \nu) / (1 + \nu)$ for plane strain or plane
108 stress state, respectively, and 109

$$\begin{aligned} h_Q &= \frac{2\tau_{12}^{\infty} (\cosh \alpha + \sinh^2 \alpha - \cos \beta) - (\sigma_{11}^{\infty} - \sigma_{22}^{\infty}) \sin \beta \sinh \alpha}{\cosh \alpha - \cos \beta} \\ &\quad + \left[2B\beta - 4K \tan^{-1} \left(\tanh \frac{\alpha}{2} \cot \frac{\beta}{2} \right) \right] (\cosh \alpha - \cos \beta) \end{aligned}$$

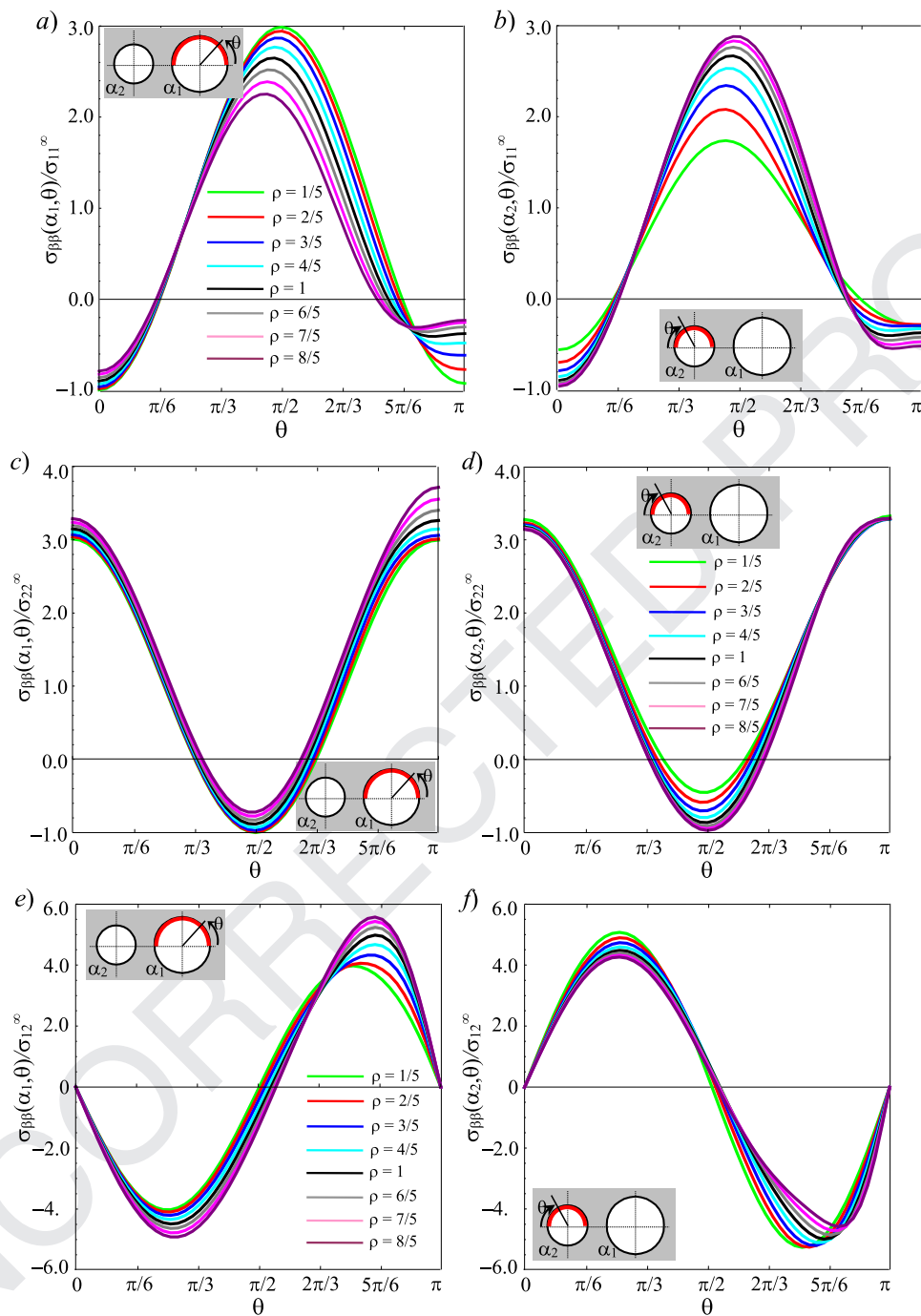


Fig. 8. Dimensionless hoop stress $\sigma_{\beta\beta}$ along the contour of the hole (a) with $\alpha = \alpha_1$ and (b) with $\alpha = \alpha_2$ for some values of ρ and $\gamma = 1$.

$$\begin{aligned}
 &+ 2(A_1 \sinh 2\alpha + C_1 \cosh 2\alpha) \sin \beta \\
 &- 2(a_1 \sinh 2\alpha + c_1 \cosh 2\alpha) \cos \beta \\
 &+ 2 \sum_{n=2}^{\infty} \{ [A_n \sinh (n+1)\alpha + B_n \sinh (n-1)\alpha \\
 &+ C_n \cosh (n+1)\alpha + D_n \cosh (n-1)\alpha] \sin n\beta + \\
 &- [a_n \sinh (n+1)\alpha + b_n \sinh (n-1)\alpha \\
 &+ c_n \cosh (n+1)\alpha + d_n \cosh (n-1)\alpha] \cos n\beta \}. \quad (2.11)
 \end{aligned}$$

110 Figs. 5–7 show distribution of the dimensionless stress fields
 111 in a plate subjected to a remote stresses σ_{11}^{∞} , σ_{22}^{∞} and σ_{12}^{∞} , re-
 112 spectively. Fig. 8 illustrates distribution of the dimensionless hoop

stress along the contours of the pores for some values of $\rho \equiv r_2/r_1$,
 113 $\gamma \equiv \delta/r_1 = 1$. Fig. 9 provides the same information for different
 114 values of γ and $\rho = 2$.
 115

3. Two overlapped circular holes

116
 117 The modeling of two overlapping circles differs considerably
 118 from the case discussed in Section 2: the circular contours rep-
 119 resent two curves of constant β ($0 \leq \beta_1 < \pi, -\pi \leq \beta_2 < 0$) for
 120 $\alpha \in (-\infty, \infty)$ (Fig. 8). In this case, Fourier transforms have to
 121 be applied instead of the Fourier series (see, for example, Ling,
 122 1947; 1948b; Dutt, 1960). The geometry of the problem is com-
 123 pletely defined by three independent parameters, e.g. coordinates

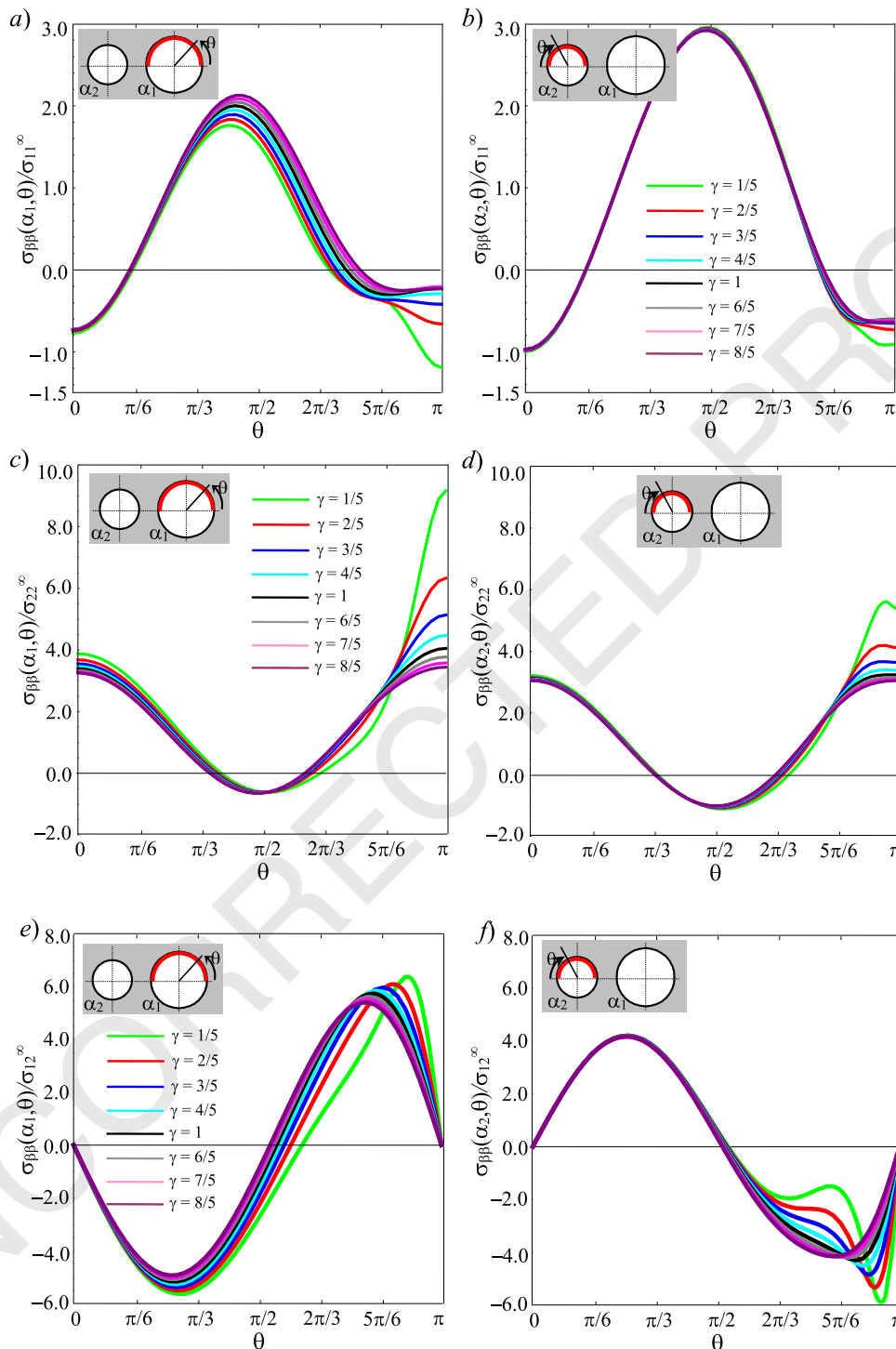


Fig. 9. Dimensionless hoop stress $\sigma_{\beta\beta}$ along the contour of the hole (a) with $\alpha = \alpha_1$ and (b) with $\alpha = \alpha_2$ for some values of γ and $\rho = 2$.

124 y_{c1}, y_{c2} of the centers of two circles and the focal distance a . Then,
 125 $\beta_1 = \arctan a/y_{c1}, \beta_2 = \arctan a/y_{c2}, r_1 = a/\sin |\beta_1|, r_2 = a/\sin |\beta_2|$,
 126 and the area included in the contour reads $A = r_1^2 (\pi - \beta_1) + r_2^2$
 127 $(\pi + \beta_2) + a^2 (\cot \beta_1 - \cot \beta_2)$. In contrast to the case of 2 sepa-
 128 rate holes, here the ligament δ turns out to be a negative quantity
 129 defined as $\delta = y_{c1} - r_1 - (y_{c2} + r_2)$.

130 The form of the fundamental stress function is the same as in
 131 (2.7), whereas the auxiliary stress functions are taken as follows:

$$h_X^{(1)} = \int_0^\infty F(s, \beta) \cos s\alpha + G(s, \beta) \sin s\alpha ds,$$

$$h_X^{(2)} = (\cosh \alpha - \cos \beta) \left\{ K \log \frac{\cosh \alpha - \cos \beta}{\cosh \alpha + \cos \beta} \right\}, \quad (3.1)$$

where

$$\begin{aligned} F(s, \beta) &= f_F(s) \sin \beta \sinh s\beta + k_F(s) \cos \beta \cosh s\beta \\ &\quad + g_F(s) \sin \beta \cosh s\beta + h_F(s) \cos \beta \sinh s\beta; \\ G(s, \beta) &= f_G(s) \sin \beta \cosh s\beta + k_G(s) \cos \beta \sinh s\beta \\ &\quad + g_G(s) \sin \beta \sinh s\beta + h_G(s) \cos \beta \cosh s\beta. \end{aligned} \quad (3.2)$$

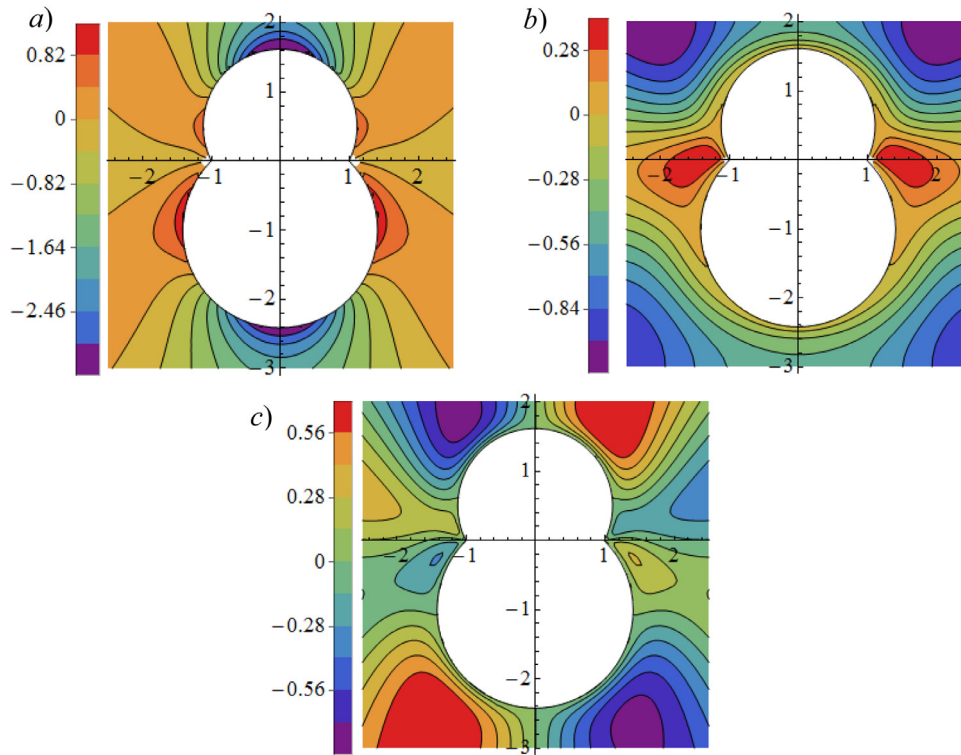


Fig. 10. Distribution of the dimensionless stress fields (a) $\sigma_{\alpha\alpha}/\sigma_{11}^{\infty}$; (b) $\sigma_{\beta\beta}/\sigma_{11}^{\infty}$; (c) $\sigma_{\alpha\beta}/\sigma_{11}^{\infty}$ in a plate subjected to a remote stress in the x_1 direction for $\kappa_1 = 1/2$ and $\kappa_2 = -1$.

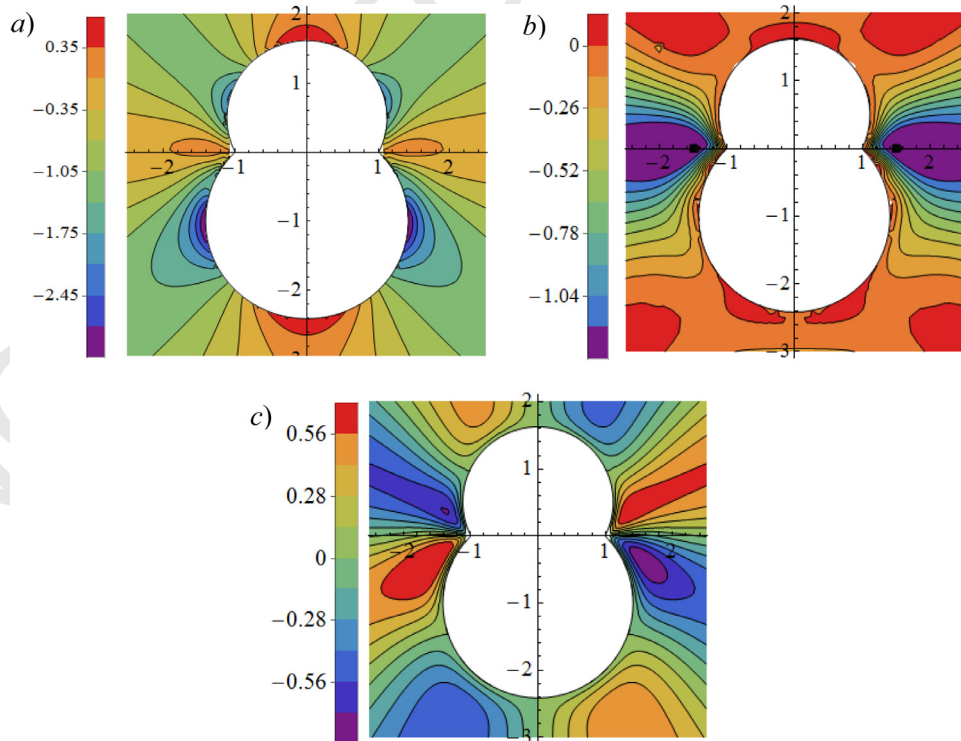


Fig. 11. Distribution of the dimensionless stress fields (a) $\sigma_{\alpha\alpha}/\sigma_{22}^{\infty}$; (b) $\sigma_{\beta\beta}/\sigma_{22}^{\infty}$; (c) $\sigma_{\alpha\beta}/\sigma_{22}^{\infty}$ in a plate subjected to a remote stress in the x_2 direction for $\kappa_1 = 1/2$ and $\kappa_2 = -1$.

133 Note also that a symmetric layout is retrieved if $\beta_2 = -\beta_1$:
 134 In such a case one has $g_F(s) = g_G(s) = h_F(s) = h_G(s) = 0$ (see
 135 Ling (1948b) for a plate with symmetric overlapped holes subjected to normal loadings and Karunes (1953) for the shear load-
 136 ing). For remotely applied shear loading it is $h_{\chi}^{(2)} = 0$.
 137

The fundamental stress function (2.7) can be rewritten, after 138
 some algebra, in the following form: 139

$$h_{\chi}^{(0)} = \frac{(\Delta\sigma^{\infty} \sin^2 \beta - 2\sigma_{12}^{\infty} \sin \beta \sinh \alpha)}{2(\cosh \alpha - \cos \beta)} + \sigma_{22}^{\infty} \cos \beta, \quad (3.3)$$

where $\Delta\sigma^{\infty} = (\sigma_{11}^{\infty} - \sigma_{22}^{\infty})$.

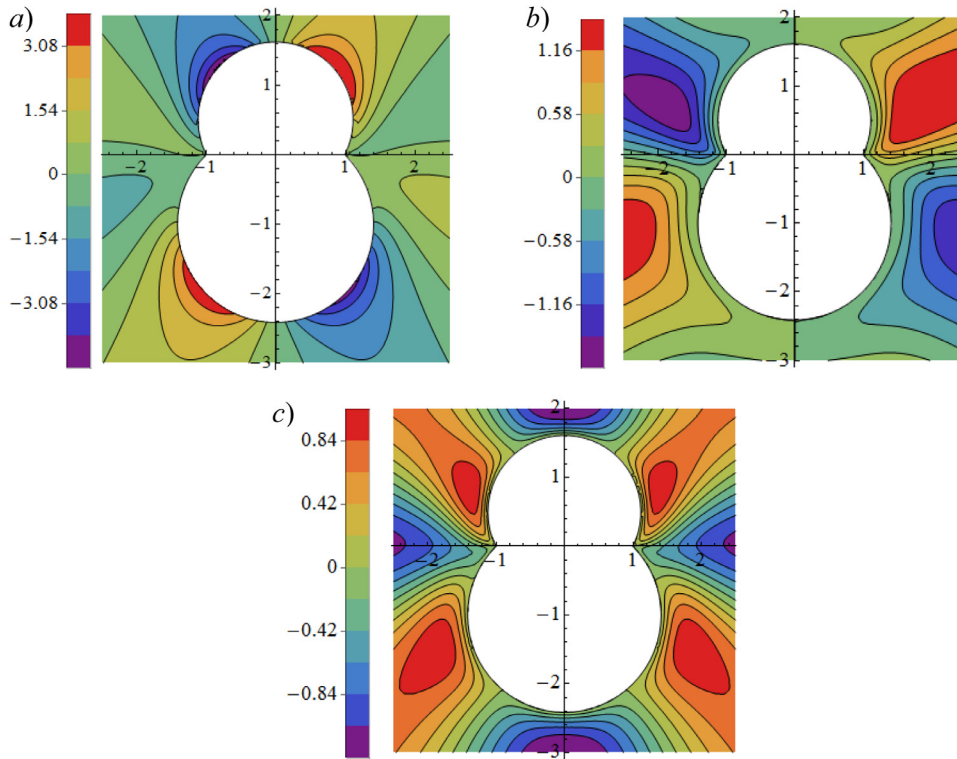


Fig. 12. Distribution of the dimensionless stress fields (a) $\sigma_{\alpha\alpha}/\sigma_{\infty 12}$; (b) $\sigma_{\beta\beta}/\sigma_{\infty 12}$; (c) $\sigma_{\alpha\beta}/\sigma_{\infty 12}$ in a plate subjected to a remote shear stress in the $x_1 \times x_2$ plane for $\kappa_1 = 1/2$ and $\kappa_2 = -1$.

141 The traction-free boundary conditions at the hole are

$$\sigma_{\beta} = 0, \quad \tau_{\alpha\beta} = 0, \quad \text{for } \beta = \beta_1, \beta_2; \\ h_{\chi}^{(1)}(\alpha, \beta) + h_{\chi}^{(2)}(\alpha, \beta) = 0 \quad \text{for } \alpha, \beta \rightarrow 0. \quad (3.4)$$

142 The first two conditions can be reformulated for the auxiliary
143 stress functions $h_{\chi}^{(1)}(\alpha, \beta)$ and $h_{\chi}^{(2)}(\alpha, \beta)$ as

$$\frac{\partial^2 h_{\chi}}{\partial \beta \partial \alpha} = 0, \quad \text{for } \beta = \beta_1, \beta_2. \quad (3.5)$$

144 and

$$\left[(\cosh \alpha - \cos \beta) \frac{\partial^2}{\partial \alpha^2} - \sinh \alpha \frac{\partial}{\partial \alpha} - \sin \beta \frac{\partial}{\partial \beta} + \cos \beta \right] \\ h_{\chi} = 0, \quad \text{for } \beta = \beta_1, \beta_2. \quad (3.6)$$

145 The last of the conditions (3.4) yields

$$\int_0^{\infty} k_F(s) ds = 0. \quad (3.7)$$

146 Taking the derivative of expression (3.6) with respect to α and
147 using (3.5) one can write

$$\frac{\partial}{\partial \alpha} \left[1 - \frac{\partial^2}{\partial \alpha^2} \right] h_{\chi} = 0, \quad \text{for } \beta = \beta_1, \beta_2, \quad (3.8)$$

148 and in turn, integration of (3.8) with respect to α gives

$$\left[1 - \frac{\partial^2}{\partial \alpha^2} \right] h_{\chi} + C_i = 0, \quad \text{for } \beta = \beta_i (i = 1, 2). \quad (3.9)$$

149 Expressions (3.5) and (3.9) can now be used to find unknown
150 functions $f_F(s), f_G(s), k_F(s), k_G(s), g_F(s)$ and $h_F(s)$. Constant K follows
151 from condition (3.7) for normal loading.

152 Condition (3.6) gives (for $\beta = \beta_1, \beta_2$).

$$\int_0^{\infty} F'(s, \beta) \sin s \alpha ds = \Delta \sigma_{\infty} \frac{(1 - \cos \beta \cosh \alpha) \sin \beta \sinh \alpha}{(\cosh \alpha - \cos \beta)^3} + B_0 \sinh \alpha$$

$$+ K \frac{\sin 2\beta \sinh 2\alpha}{(\cosh \alpha + \cos \beta)^2 (\cosh \alpha - \cos \beta)}; \\ \int_0^{\infty} s G'(s, \beta) \cos s \alpha ds = -\sigma_{12}^{\infty} \frac{(3 - 4 \cos \beta \cosh \alpha + \cos 2\beta \cosh 2\alpha)}{2(\cosh \alpha - \cos \beta)^3}, \quad (3.10)$$

153 where the apex denotes derivative with respect to coordinate β
154 whereas from condition (3.9) one has

$$\int_0^{\infty} (1 + s^2) F(s, \beta) \cos s \alpha ds = K \cos \beta \ln \frac{\cosh \alpha - \cos \beta}{\cosh \alpha + \cos \beta} + 2K \cos \beta \\ + 2K \frac{\cos^2 \beta}{\cosh \alpha + \cos \beta} - K \frac{\sin^2 2\beta}{(\cosh \alpha - \cos \beta)(\cos \alpha + \cos \beta)^2} \\ - \frac{\sigma_{11}^{\infty} \sin^2 \beta}{2} \left(\frac{1}{\cosh \alpha - \cos \beta} + \frac{\cosh \alpha}{(\cosh \alpha - \cos \beta)^2} + \right. \\ \left. - \frac{2 \sinh^2 \alpha}{(\cosh \alpha - \cos \beta)^3} \right) - \frac{\sigma_{22}^{\infty}}{2} \left(-\frac{2 \cosh^2 \alpha + \sinh^2 \alpha}{(\cosh \alpha - \cos \beta)} \right. \\ \left. + \frac{5 \cosh \alpha \sinh^2 \alpha}{(\cosh \alpha - \cos \beta)^2} - \frac{2 \sinh^4 \alpha}{(\cosh \alpha - \cos \beta)^3} \right) - C_i; \\ \int_0^{\infty} (1 + s^2) G(s, \beta) \sin s \alpha ds = +\sigma_{12}^{\infty} \frac{3 \cosh \alpha \sinh \alpha \sin \beta}{(\cosh \alpha - \cos \beta)^2} \\ - \sigma_{12}^{\infty} \frac{2 \sin \beta \sinh^3 \alpha}{(\cosh \alpha - \cos \beta)^3} - \tilde{C}_i; \quad (3.11)$$

Eq. (3.11)_{1,2} for $\alpha \rightarrow \infty$ yield

$$C_i = [2K - \sigma_{22}^{\infty} + B_0 \beta] \cos \beta, \quad \tilde{C}_i = \sigma_{12}^{\infty} \sin \beta, \quad \text{for } \beta = \beta_i (i = 1, 2). \quad (3.12)$$

156 Thus, from Eqs. (3.10) and (3.11), taking into account results
157 (3.12) one has for $\beta = \beta_i$ ($i = 1, 2$)

$$F'(s, \beta_i) = \frac{2a\Delta\sigma^\infty}{s\pi} \int_0^\infty \sin s\alpha \frac{(1 - \cos\beta \cosh\alpha) \sin\beta \sinh\alpha}{(\cosh\alpha - \cos\beta)^3} d\alpha$$

$$+ \frac{2K}{s\pi} \int_0^\infty \sin s\alpha \frac{\sin 2\beta \sinh 2\alpha}{(\cosh\alpha + \cos\beta)^2 (\cosh\alpha - \cos\beta)} d\alpha;$$

$$G'(s, \beta_i) = -\sigma_{12}^\infty \frac{2}{s\pi}$$

$$\int_0^\infty \frac{(3 - 4\cos\beta \cosh\alpha + \cos 2\beta \cosh 2\alpha)}{2(\cosh\alpha - \cos\beta)^3} \cos s\alpha d\alpha \quad (3.13)$$

158 and

$$F(s, \beta_i) = \frac{2K}{(1+s^2)\pi} \cos\beta \int_0^\infty \cos s\alpha \ln \frac{\cosh\alpha - \cos\beta}{\cosh\alpha + \cos\beta} d\alpha$$

$$+ \frac{4K}{(1+s^2)\pi} \cos^2\beta \int_0^\infty \frac{\cos s\alpha}{\cosh\alpha + \cos\beta} d\alpha +$$

$$- \frac{2K}{(1+s^2)\pi} \sin^2 2\beta \int_0^\infty \frac{\cos s\alpha}{(\cosh\alpha - \cos\beta)(\cosh\alpha + \cos\beta)^2} d\alpha +$$

$$+ a \frac{\Delta\sigma^\infty}{(1+s^2)\pi} \sin^2\beta \int_0^\infty \cos s\alpha \left(\frac{3\cos\beta}{(\cos\alpha - \cos\beta)^2} \right.$$

$$\left. - \frac{2\sin^2\beta}{(\cos\alpha - \cos\beta)^3} \right) d\alpha;$$

$$G(s, \beta_i) = -\frac{2\sigma_{12}^\infty}{(1+s^2)\pi} \sin\beta \int_0^\infty \sin s\alpha d\alpha$$

$$+ \frac{6\sigma_{12}^\infty}{(1+s^2)\pi} \sin\beta \int_0^\infty \frac{\cosh\alpha \sinh\alpha \sin s\alpha}{(\cosh\alpha - \cos\beta)^2} d\alpha +$$

$$- \frac{4\sigma_{12}^\infty}{(1+s^2)\pi} \sin\beta \int_0^\infty \frac{\sinh^3\alpha \sin s\alpha}{(\cosh\alpha - \cos\beta)^3} d\alpha. \quad (3.14)$$

159 Note that, through the results reported in Appendix A2, all the
160 Fourier transforms involved in the Eqs. (3.13) and (3.14) can be
161 evaluated in closed form, thus allowing to find the analytic expres-
162 sions of functions $F(s, \beta)$, $G(s, \beta)$ and their derivatives:

$$F(s, \beta) = -2K \cos\beta \frac{\sinh s(\frac{\pi}{2} - |\beta|)}{s(1+s^2) \cosh \frac{s\pi}{2}} + 4K \cos^2\beta \frac{\sinh s\beta}{(1+s^2) \sinh s\pi \sin\beta}$$

$$- a\Delta\sigma^\infty \sin^2\beta \csc|\beta| \operatorname{cschs}\pi \sinh s(\pi - |\beta|) +$$

$$- K \sin^2 2\beta \frac{\sec\beta \sinh s(\pi - |\beta|) - 2s \cosh s\beta \csc|\beta| - (-2 \cot\beta \csc\beta + \sec|\beta|) \sinh s|\beta|}{2(1+s^2) \sin|\beta| \cos\beta \sinh s\pi};$$

$$G(s, \beta) = 2\sigma_{12}^\infty \frac{\pi s(1+s^2) \cosh s(\pi - |\beta|) \operatorname{cschs}(\pi s) - 1}{s\pi(1+s^2)} \sin|\beta|;$$

$$F'(s, \beta) = 4K \sin 2\beta \frac{s \cos\beta \sinh s|\beta| + \sinh \frac{s\pi}{2} \sinh s(\frac{\pi}{2} - |\beta|) \sin|\beta|}{s \sin|2\beta| \sinh s\pi}$$

$$+ a\Delta\sigma^\infty \sin\beta \frac{s(\cosh s(\pi - |\beta|) - \sinh s(\pi - |\beta|) \cot|\beta|)}{s \sinh s\pi};$$

$$G'(s, \beta) = 2\sigma_{12}^\infty \operatorname{cschs}\pi [\cos\beta \cosh s(\pi - |\beta|) - s \sin|\beta| \sinh s(\pi - |\beta|)]. \quad (3.15)$$

163 System (3.15) imposed for $\beta = \beta_i$ ($i = 1, 2$) allows assessing
164 functions $f_F(s)$, $f_G(s)$, $k_F(s)$, $k_G(s)$, $g_F(s)$, $g_G(s)$, $h_F(s)$ and $h_G(s)$ and, in
165 turn, the stress and displacement fields according to Eqs. (2.4) and
166 (2.10), respectively. For the case of two equal overlapping holes
167 $\beta_1 = -\beta_2$ the expressions of $f_F(s)$, $k_F(s)$ reported in Ling (1948b) for
168 normal loadings and $f_G(s)$, $k_G(s)$ reported in Karunes (1953) for
169 shear loadings are exactly retrieved (actually, a misprint occurred
170 in expression (16)₁ of F_n reported in Karunes (1954), in which the
171 square in “ n^2 ” must be removed). Figs. 10–12 illustrate distribution
172 of the dimensionless stress fields in a plate subjected to a remote
173 stresses σ_{11}^∞ , σ_{22}^∞ and σ_{12}^∞ , respectively.

4. Evaluation of the compliance contribution tensor

175

Compliance contribution tensors have been first introduced by
Horii and Nemat-Nasser (1983) for pores of ellipsoidal shape (ex-
plicit formulas connecting compliance contribution tensor and Es-
helby tensor for an ellipsoidal pore are given in the appendix of
the mentioned paper). Components of this tensor for various two-
dimensional pores were given by Kachanov et al. (1994) and for
ellipsoidal inhomogeneities – by Sevostianov and Kachanov (1999).
This tensor connects the extra strain due to the presence of the in-
homogeneity under given remotely applied stresses. Indeed, if we
consider a representative volume element V containing an isolated
inhomogeneity of volume V_1 , the average, over representative vol-
ume V strain can be represented as a sum

$$\boldsymbol{\varepsilon} = \mathbf{S}^0 : \boldsymbol{\sigma}^0 + \Delta\boldsymbol{\varepsilon} \quad (4.1)$$

where \mathbf{S}^0 is the compliance tensor of the matrix and $\boldsymbol{\sigma}^0$ represents
the uniform boundary conditions (tractions on ∂V have the form
 $\mathbf{t}|_{\partial V} = \boldsymbol{\sigma}^0 \cdot \mathbf{n}$ where $\boldsymbol{\sigma}^0$ is a constant tensor); $\boldsymbol{\sigma}^0$ can be viewed as
far-field (“remotely applied”) stress. The material is assumed to be
linear elastic; hence the extra strain due to the inhomogeneity $\Delta\boldsymbol{\varepsilon}$
is a linear function of $\boldsymbol{\sigma}^0$:

$$\Delta\boldsymbol{\varepsilon} = \frac{V_1}{V} \mathbf{H} : \boldsymbol{\sigma}^0 \quad (4.2)$$

where \mathbf{H} is a fourth-rank compliance contribution tensor of the
inhomogeneity. If the inhomogeneity is a pore, the extra overall
strain due its presence is given by the well-known expression in
terms of an integral over the pore boundary (Hill, 1963):

$$\Delta\boldsymbol{\varepsilon} = \frac{1}{2V} \int_{\partial V} (\mathbf{un} + \mathbf{nu}) dS \quad (4.3)$$

Thus, Neumann boundary value problem has to be solved in order
to find the compliance contribution tensor of a pore.

4.1. Two separate circular inhomogeneities (symmetric with respect
to x_1 axis)

The components of the unit vector and the infinitesimal arc
length on the contour of the two circles with $\alpha = \text{const}$ are:

$$n_1 = -\frac{\cosh\alpha_i \cos\beta - 1}{\cosh\alpha_i - \cos\beta} \operatorname{sign}(\alpha_i), \quad n_2 = -\frac{\sinh|\alpha_i| \sin\beta}{\cosh\alpha_i - \cos\beta}$$

$$ds = r_i d\theta = \frac{a \operatorname{sign}(\alpha_i)}{\cosh\alpha_i - \cos\beta} d\beta, \quad i = 1, 2 \quad (4.4)$$

where θ is the polar angle measured from x_1 axis as shown in
Fig. 13(a). In the Cartesian coordinate system (x_1, x_2), the compo-
nents of the unit vector, the displacement field and the infinitesi-
mal arc length on the contour of the two separate circles with

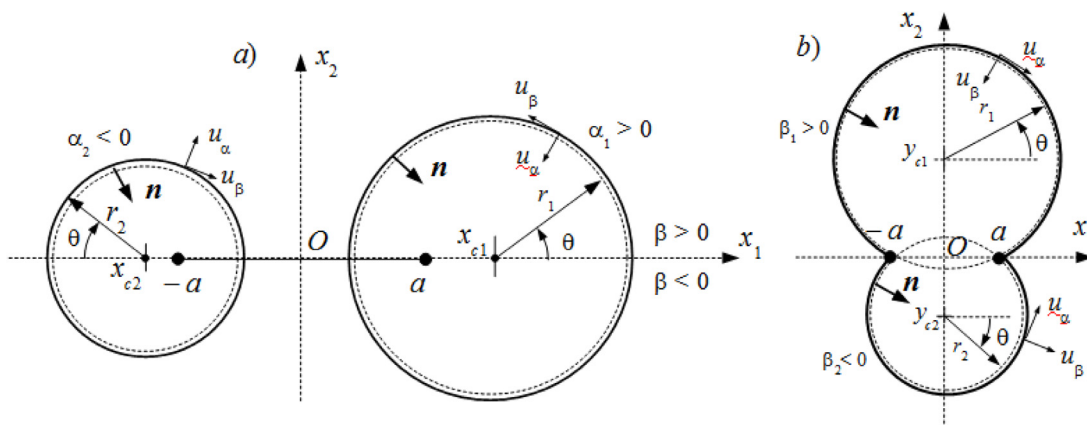


Fig. 13. Sketch of the polar coordinate systems used to perform the circular integrals involved in expression (4.2) for the components of the extra overall strain.

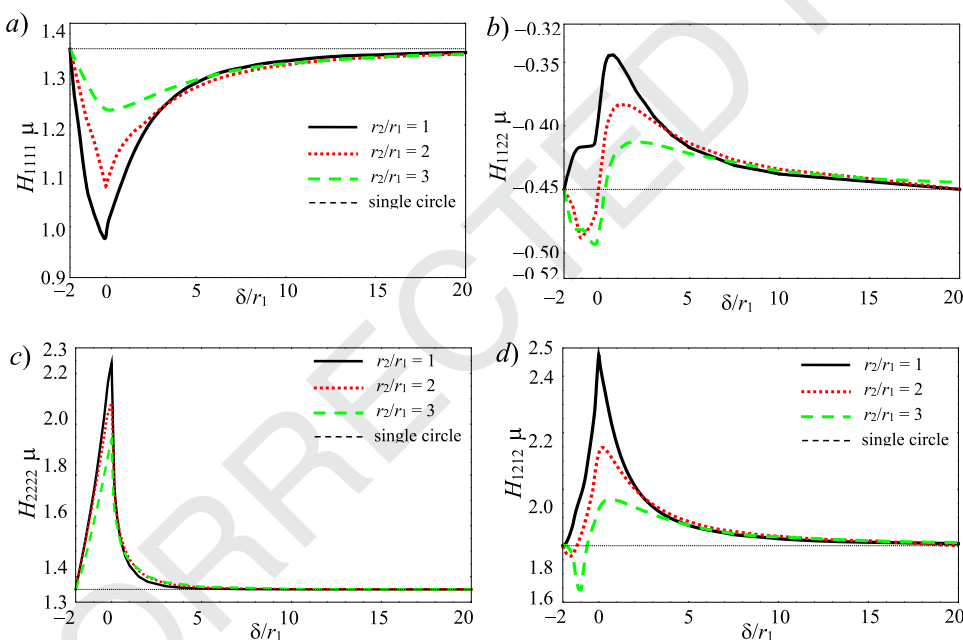


Fig. 14. Normalized components of the cavity compliance tensor (a) $H_{1111} \mu$; (b) $H_{1122} \mu$; (c) $H_{2222} \mu$; (d) $H_{1212} \mu$ for some values of ρ . Reference is made to plane strain condition.

208 $\alpha = \text{const}$ are

$$u_1 = -u_\alpha \cos \theta - u_\beta \sin \theta; \quad u_2 = -u_\alpha \sin \theta + u_\beta \cos \theta; \quad (4.5)$$

209 with

$$\cos \theta = \frac{\cosh \alpha_i \cos \beta - 1}{\cosh \alpha_i - \cos \beta} \text{sign}(\alpha_i); \quad \sin \theta = \frac{\sinh |\alpha_i| \sin \beta}{\cosh \alpha_i - \cos \beta};$$

$$ds = r_i d\theta = \frac{a \text{sign}(\alpha_i)}{\cosh \alpha_i - \cos \beta} d\beta. \quad (4.6)$$

210 and

$$\text{for } \alpha = \alpha_1 > 0: \quad n_1 = -\cos \theta; \quad n_2 = -\sin \theta;$$

$$\text{for } \alpha = \alpha_1 < 0: \quad n_1 = \cos \theta; \quad n_2 = -\sin \theta. \quad (4.7)$$

211 Now, using results of the Section 2 and formulas (4.3) compli-
212 ance contribution tensor can be calculated for two separate pores
213 (the integral has to be evaluated numerically).

4.2. Overlapped circles symmetric with respect to x_2 axis 214

The component of the unit vector and the infinitesimal arc 215
length on the contour at $\beta = \text{const}$ are 216

$$n_1 = -\frac{\sinh \alpha \sin \beta_i \text{sign}(\beta_i)}{\cosh \alpha - \cos \beta_i}; \quad n_2 = -\frac{1 - \cosh \alpha \cos \beta_i \text{sign}(\beta_i)}{\cosh \alpha - \cos \beta_i}$$

$$ds = r_i d\theta = -\frac{a \text{sign}(\beta_i)}{\cosh \alpha - \cos \beta_i} d\alpha, \quad i = 1, 2 \quad (4.8)$$

For the overlapping holes (Fig. 13(b)), one finds 217

$$u_1 = u_\alpha \sin \theta - u_\beta \cos \theta; \quad u_2 = -u_\alpha \cos \theta - u_\beta \sin \theta; \quad (4.9)$$

$$\text{for } \beta = \beta_1 > 0: \quad n_1 = -\cos \theta; \quad n_2 = -\sin \theta;$$

$$\text{for } \beta = \beta_2 < 0: \quad n_1 = -\cos \theta; \quad n_2 = \sin \theta; \quad (4.10)$$

$$\cos \theta = \frac{\sinh \alpha \sin \beta_i}{\cosh \alpha - \cos \beta_i}; \quad \sin \theta = \frac{1 - \cosh \alpha \cos \beta_i}{\cosh \alpha - \cos \beta_i},$$

$$ds = r_i d\theta = -\frac{a \operatorname{sign}(\beta_i)}{\cosh \alpha - \cos \beta_i} d\alpha. \quad (4.11)$$

220 Taking into account that the area of the pore cross-section $A_i =$
 221 $r_i^2(\pi - |\beta_i + (\sin |2\beta_1|)/2|)$, one can use results of Section 3 and
 222 formula (4.3) to evaluate the compliance contribution tensor.

223 Fig. 14 illustrates the dimensionless components of the compli-
 224 ance contribution tensor in dependence on δ/r_1 for different values
 225 of r_2/r_1 .

226 **5. Concluding remarks**

227 In this paper, we calculated compliance contribution tensor of
 228 two separate or intersecting circular pores. For this goal, we first
 229 considered two holes and solved Neumann boundary value prob-
 230 lem in two-steps: (1) assessment of the fundamental displacement
 231 field related to a remotely applied uniform stress in a homoge-
 232 neous body and (2) fulfillment of the boundary conditions in the
 233 problem with pores by adding an extra-term to the fundamental
 234 field. This solution was used to construct the compliance contribu-
 235 tion tensor of the combination of two circular pores by calculating
 236 proper contour integrals. Plots for H_{1111} and H_{2222} (Fig. 14(a) and
 237 (c)) generally reproduce the curves for two corresponding compo-
 238 nents of the resistivity contribution tensor (Lanzoni et al., 2018). At
 239 the same time, components H_{1122} and H_{1212} behave differently and
 240 may show non-monotonic not only near $\delta/r_1 = 1$ (point where the
 241 circles touch each other), but also when $\delta/r_1 > 1$ or $\delta/r_1 < 1$ (see
 242 Fig. 14(b) and (d)). This is in agreement with expressions for cross-
 243 property connections for a material with ellipsoidal/elliptical pores
 244 and inhomogeneities derived by Sevostianov and Kachanov (2002,
 245 2008). In particular, for a two-dimensional elliptical hole

$$\mathbf{H} = \frac{1}{E_0} \left[\frac{(2a_2 + a_1)}{a_1} \mathbf{e}_1 \mathbf{e}_1 \mathbf{e}_1 \mathbf{e}_1 + \frac{(2a_1 + a_2)}{a_2} \mathbf{e}_2 \mathbf{e}_2 \mathbf{e}_2 \mathbf{e}_2 + \frac{(a_1 + a_2)^2}{2a_1 a_2} (\mathbf{e}_1 \mathbf{e}_2 + \mathbf{e}_2 \mathbf{e}_1)(\mathbf{e}_1 \mathbf{e}_2 + \mathbf{e}_2 \mathbf{e}_1) - (\mathbf{e}_1 \mathbf{e}_1 \mathbf{e}_2 \mathbf{e}_2 + \mathbf{e}_2 \mathbf{e}_2 \mathbf{e}_1 \mathbf{e}_1) \right] \quad (5.1)$$

246
$$\mathbf{R} = \frac{1}{k_0} \left(\frac{a_1 + a_2}{a_1} \mathbf{e}_1 \mathbf{e}_1 + \frac{a_1 + a_2}{a_2} \mathbf{e}_2 \mathbf{e}_2 \right) \quad (5.2)$$

247 So that

$$E_0 H_{1111} = k_0 R_{11} \left[1 + \frac{1}{k_0 R_{22}} \right]; \quad E_0 H_{2222} = k_0 R_{22} \left[1 + \frac{1}{k_0 R_{11}} \right];$$

$$E_0 H_{1212} = \frac{1}{k_0 R_{11}} + \frac{1}{k_0 R_{22}}; \quad E_0 H_{1122} = \frac{(R_{11} + R_{22})^2}{R_{11} R_{22}} \quad (5.3)$$

248 Components R_{11} and R_{22} that behave oppositely (one increases
 249 when another decreases) enter expressions for H_{1122} and H_{1212} in
 250 concurrent manner, so that their combined effect may be quite
 251 complex.

252 The case $\delta/r_1 = -2$, $r/r_1 = 1$ corresponds to an isolated circular
 253 inhomogeneity. In this case, the well-known result for the compli-
 254 ance contribution tensor of a circular hole (see Horii and Nemat-
 255 Nasser, 1983) is recovered. The compliance contribution tensor
 256 constitutes the basic building block for calculation of the overall
 257 elastic properties of a material containing parallel cylindrical holes
 258 with the cross-sections shown in Fig. 2 (see Kachanov and Sevostianov, 2018)

260 **Acknowledgments**

261 Financial support from the Italian Ministry of Education, Uni-
 262 versity and Research (MIUR) in the framework of the Project PRIN
 263 2017 Modelling of constitutive laws for traditional and innovative
 264 building materials (code 2017HFPKZY) is gratefully acknowledged.
 265 IS and ER acknowledge financial support of Indam-GNFM "Gruppo
 266 Nazionale per la Fisica Matematica".

Appendices

A1. Integration constants used in Section 2

$$A_1 = \frac{1}{D} \cosh(\alpha_1 + \alpha_2) \{ 2f(\alpha_1) \sinh^2 \alpha_2 - 2f(\alpha_2) \sinh^2 \alpha_1 + [g(\alpha_1) - g(\alpha_2)] \tanh(\alpha_1 + \alpha_2) \}, \quad (A1.1)$$

$$B_1 = \frac{1}{D} \cosh(\alpha_1 - \alpha_2) \{ 2f(\alpha_2) \sinh^2 \alpha_1 - 2f(\alpha_1) \sinh^2 \alpha_2 - [g(\alpha_1) + g(\alpha_2)] \tanh(\alpha_1 - \alpha_2) + g(\alpha_2) \sinh 2\alpha_1 - g(\alpha_1) \sinh 2\alpha_2 \} \quad (A1.2)$$

$$C_1 = \frac{1}{D} \cosh(\alpha_1 + \alpha_2) \{ g(\alpha_2) - g(\alpha_1) + [f(\alpha_1) - f(\alpha_2)] \tanh(\alpha_1 + \alpha_2) + f(\alpha_2) \sinh 2\alpha_1 - f(\alpha_1) \sinh 2\alpha_2 \} \quad (A1.3)$$

$$B = B = \frac{2}{D} \cosh(\alpha_1 - \alpha_2) \{ [f(\alpha_1) + f(\alpha_2)] \tanh(\alpha_1 - \alpha_2) + g(\alpha_2) - g(\alpha_1) \}, \quad (A1.4)$$

where:

$$f(\alpha) = 2K e^{-|\alpha|} \sinh \alpha - (\sigma_{22}^\infty - \sigma_{11}^\infty) e^{-2|\alpha|} \operatorname{sign} \alpha, \\ g(\alpha) = \cosh 2\alpha - e^{-|\alpha|} (\sigma_{11}^\infty \cosh \alpha + \sigma_{22}^\infty \sinh |\alpha|), \quad (A1.5)$$

$$D = 2 \sinh(\alpha_1 - \alpha_2) (\sinh^2 \alpha_1 + \sinh^2 \alpha_2) \quad (A1.6)$$

$$a_1 = \tau_{12}^\infty \frac{e^{-2|\alpha_1|} \cosh 2\alpha_2 - e^{-2|\alpha_2|} \cosh 2\alpha_1}{\sinh 2(\alpha_1 - \alpha_2)}, \quad (A1.7)$$

$$c_1 \tau_{12}^\infty \frac{e^{-2|\alpha_1|} \sinh 2\alpha_2 + e^{-2|\alpha_2|} \sinh 2\alpha_1}{\sinh 2(\alpha_1 - \alpha_2)}. \quad (A1.8)$$

$$A_n = \frac{1}{H_n} \{ P_n(\alpha_1, \alpha_2) \Phi_n(\alpha_1) + P_n(\alpha_2, \alpha_1) \Phi_n(\alpha_2) + Q_n(\alpha_1, \alpha_2) \Phi_n^*(\alpha_1) + Q_n(\alpha_2, \alpha_1) \Phi_n^*(\alpha_2) \} \quad (A1.9)$$

$$B_n = \frac{1}{H_n} \{ P_{-n}(\alpha_1, \alpha_2) \Phi_n(\alpha_1) + P_{-n}(\alpha_2, \alpha_1) \Phi_n(\alpha_2) + Q_{-n}(\alpha_1, \alpha_2) \Phi_n^*(\alpha_1) + Q_{-n}(\alpha_2, \alpha_1) \Phi_n^*(\alpha_2) \} \quad (A1.10)$$

$$C_n = -\frac{1}{H_n} \{ U_n(\alpha_1, \alpha_2) \Phi_n(\alpha_1) + U_n(\alpha_2, \alpha_1) \Phi_n(\alpha_2) + [V_n(\alpha_1, \alpha_2) + \cosh(2n\alpha_2 - (n-1)\alpha_1)] \Phi_n^*(\alpha_1) + V_n(\alpha_2, \alpha_1) \Phi_n^*(\alpha_2) \} \quad (A1.10A)$$

$$D_n = \frac{1}{H_n} \{ U_{-n}(\alpha_1, \alpha_2) \Phi_n(\alpha_1) + U_{-n}(\alpha_2, \alpha_1) \Phi_n(\alpha_2) + V_{-n}(\alpha_1, \alpha_2) \Phi_n^*(\alpha_1) + V_{-n}(\alpha_2, \alpha_1) \Phi_n^*(\alpha_2) \} \quad (A1.11)$$

$$a_n = \frac{1}{H_n} \{ P_n(\alpha_1, \alpha_2) \Psi_n(\alpha_1) + P_n(\alpha_2, \alpha_1) \Psi_n(\alpha_2) + Q_n(\alpha_1, \alpha_2) \Psi_n^*(\alpha_1) + Q_n(\alpha_2, \alpha_1) \Psi_n^*(\alpha_2) \} \quad (A1.12)$$

$$b_n = \frac{1}{H_n} \{P_{-n}(\alpha_1, \alpha_2)\Psi_n(\alpha_1) + P_{-n}(\alpha_2, \alpha_1)\Psi_n(\alpha_2) + Q_{-n}(\alpha_1, \alpha_2)\Psi_n^*(\alpha_1) + Q_{-n}(\alpha_2, \alpha_1)\Psi_n^*(\alpha_2)\} \quad (A1.13)$$

$$c_n = -\frac{1}{H_n} \{U_n(\alpha_1, \alpha_2)\Psi_n(\alpha_1) + U_n(\alpha_2, \alpha_1)\Psi_n(\alpha_2) + [V_n(\alpha_1, \alpha_2) + \cosh(2n\alpha_2 - (n-1)\alpha_1)]\Psi_n^*(\alpha_1) + V_n(\alpha_2, \alpha_1)\Psi_n^*(\alpha_2)\} \quad (A1.14)$$

$$d_n = \frac{1}{H_n} \{U_{-n}(\alpha_1, \alpha_2)\Psi_n(\alpha_1) + U_{-n}(\alpha_2, \alpha_1)\Psi_n(\alpha_2) + V_{-n}(\alpha_1, \alpha_2)\Psi_n^*(\alpha_1) + V_{-n}(\alpha_2, \alpha_1)\Psi_n^*(\alpha_2)\} \quad (A1.15)$$

for $n \geq 2$, where

$$P_n(\xi, \eta) = \frac{1}{n+1} (\sinh(\xi+n\eta) \sinh n(\xi-\eta) + n \sinh(\xi+n\xi) \sinh(\xi-\eta)), \quad (A1.16)$$

$$Q_n(\xi, \eta) = \cosh(\xi+n\eta) \sinh n(\xi-\eta) - n \cosh(\eta+n\xi) \sinh(\xi-\eta), \quad (A1.17)$$

$$U_n(\xi, \eta) = \frac{1}{n+1} [\cosh(\xi+n\eta) \sinh n(\xi-\eta) + n \cosh(\eta+n\xi) \sinh(\xi-\eta)], \quad (A1.18)$$

$$V_n(\xi, \eta) = \sinh(\xi+n\eta) \sinh n(\xi-\eta) - n \sinh(\eta+n\xi) \sinh(\xi-\eta), \quad (A1.19)$$

$$H_n = 2n \{ \sinh^2[n(\alpha_1 - \alpha_2)] - n^2 \sinh^2(\alpha_1 - \alpha_2) \}. \quad (A1.20)$$

$$\Phi_n^*(\alpha) = 2K e^{-n|\alpha|} \sinh \alpha - (\sigma_{22}^\infty - \sigma_{11}^\infty) n g_n(\alpha) \text{sign} \alpha, \quad (A1.21)$$

$$\Phi_n(\alpha) = -e^{-n|\alpha|} [2K (\cosh \alpha + n \text{sign}|\alpha|) + (\sigma_{22}^\infty - \sigma_{11}^\infty) n (n^2 - 1) \sinh|\sigma_{22}^\infty|] \quad (A1.22)$$

$$\int_0^\infty \frac{\cos s\alpha}{(\cosh \alpha - \cos \beta)(\cosh \alpha + \cos \beta)^2} d\alpha = \pi \frac{\sec|\beta| \sinh s(\pi - |\beta|) \cos \beta - 2s \cosh s\beta \csc \beta - (\sec|\beta| - 2 \cot|\beta| \csc \beta) \sinh s|\beta|}{4 \sin|\beta| \cos \beta \sinh s\pi}; \quad (A2.9)$$

$$\Psi_n^*(\alpha) = 2n g_n(\alpha) \quad (A1.23)$$

$$\Psi_n(\alpha) = 2 \tau_{12}^\infty n (n^2 - 1) e^{-n|\alpha|} \sinh \alpha. \quad (A1.24)$$

Finally, the constant K follows from the condition

$$\sum_{n=1}^\infty (A_n + B_n) = 0. \quad (A1.25)$$

after the introduction of the constants A_n and B_n , for $n \geq 1$.

A2. Useful Fourier transforms

The following definite integrals have been used to find expressions (3.13) and (3.14):

$$\int_0^\infty \frac{(1 - \cos \beta \cosh \alpha) \sinh \alpha}{(\cosh \alpha - \cos \beta)^3} \sin s\alpha ds = \frac{\pi}{2} s \frac{(s \cosh s(\pi - |\beta|) - \sinh s(\pi - |\beta|) \cot|\beta|)}{\sinh s\pi}; \quad (A2.1)$$

$$\int_0^\infty \frac{\sinh 2\alpha}{(\cosh \alpha - \cos \beta)(\cosh \alpha + \cos \beta)^2} \sin s\alpha ds = 2\pi \frac{s \sinh s|\beta| \cos \beta + \sinh \frac{s\pi}{2} \sinh s(\frac{\pi}{2} - |\beta|) \sin|\beta|}{\sinh s\pi \sin 2|\beta|}; \quad (A2.2)$$

$$\int_0^\infty \frac{\cos s\alpha}{(\cosh \alpha - \cos \beta_1)} d\alpha = \pi \frac{\sinh s(\pi - |\beta_1|)}{\sinh s\pi \sin|\beta_1|}; \quad (A2.3)$$

$$\int_0^\infty \frac{\cos s\alpha}{(\cosh \alpha + \cos \beta_1)} d\alpha = \pi \frac{\sinh s|\beta_1|}{\sinh s\pi \sin|\beta_1|}; \quad (A2.4)$$

$$\int_0^\infty \frac{\cos s\alpha}{(\cosh \alpha + \cos \beta_1)^2} d\alpha = \pi \frac{s \cosh \beta_1 - \cot|\beta_1| \sinh s|\beta_1|}{\sinh s\pi \sin^2|\beta_1|}; \quad (A2.5)$$

$$\int_0^\infty \log\left(\frac{\cosh \alpha - \cos \beta_1}{\cosh \alpha + \cos \beta_1}\right) \cos s\alpha d\alpha = -\pi \frac{\sinh s(\frac{\pi}{2} - |\beta_1|)}{s \cosh(s\frac{\pi}{2})}; \quad (A2.6)$$

$$\int_0^\infty \frac{\cos s\alpha}{(\cosh \alpha - \cos \beta_1)^2} d\alpha = \pi \frac{s \cosh s(\pi - |\beta_1|) + \cot|\beta_1| \sinh s(\pi - |\beta_1|)}{\sin^2 \beta_1 \sinh s\pi}; \quad (A2.7)$$

$$\int_0^\infty \frac{\cos s\alpha}{(\cosh \alpha - \cos \beta_1)^3} d\alpha = \pi \frac{3s \cosh s(\pi - |\beta_1|) \cot|\beta_1| + (s^2 - 2 + 3\csc^2 \beta_1) \sinh s(\pi - |\beta_1|)}{\sin^3 |\beta_1| \sinh s\pi}; \quad (A2.8)$$

$$\int_0^\infty \frac{\cosh \alpha}{(\cosh \alpha - \cos \beta_1)} \cos(s\alpha) d\alpha = \pi \frac{\sinh s(\pi - |\beta_1|) \cos \beta_1}{\sinh s\pi \sin|\beta_1|}; \quad (A2.10)$$

$$\int_0^\infty \frac{\cosh \alpha}{(\cosh \alpha - \cos \beta_1)^2} \cos(s\alpha) d\alpha = \pi \frac{s \cosh s(\pi - |\beta_1|) \cot|\beta_1| + \csc^2 |\beta_1| \sinh s(\pi - |\beta_1|)}{\sinh s\pi \sin|\beta_1|}; \quad (A2.11)$$

$$\int_0^\infty \frac{\sinh \alpha}{(\cosh \alpha - \cos \beta_1)^2} \sin(s\alpha) d\alpha = s\pi \frac{\sinh s\pi \cosh s\beta_1 - \cosh s\pi \sinh |s\beta_1|}{\sinh s\pi \sin|\beta_1|}; \quad (A2.12)$$

308

$$\int_0^{\infty} \frac{\cos s\alpha}{(\cosh \alpha - \cos \beta_1)^2} d\alpha$$

$$= \pi \frac{\cosh s\beta_1 (s \coth s\pi + \cot |\beta_1|) - \sinh s|\beta_1| (s + \cot |\beta_1| \coth s\pi)}{\sin^2 \beta_1}; \quad (\text{A2.13})$$

309 **References**

- 310 Drenchev, L., Sobczak, J., 2009. Gasars. A specific Class of Porous Materials. Motor
311 Transport Institute, Krakow.
- 312 Dutt, S.B., 1960. On the stresses due to an overlapped circular hole on the neutral
313 axis of a deep beam under constant bending moment. Appl. Sci. Res. 9, 457–
314 462.
- 315 Ekneligoda, T.C., Zimmerman, R.W., 2006. Compressibility of two-dimensional pores
316 having n-fold axes of symmetry. Proc. R. Soc. A 462, 1933–1947.
- 317 Ekneligoda, T.C., Zimmerman, R.W., 2008b. Boundary perturbation solution for
318 nearly-circular holes and rigid inclusions in an infinite elastic medium. ASME
319 J. Appl. Mech. 75 paper 011015-1.
- 320 Ekneligoda, T.C., Zimmerman, R.W., 2008a. Shear compliance of two-dimensional
321 pores possessing N-fold axis of rotational symmetry. Proc. R. Soc. A 464, 759–
322 775.
- 323 Hill, R., 1963. Elastic properties of reinforced solids: some theoretical principles.
324 J. Mech. Phys. Solids 11, 357–372.
- 325 Horii, H., Nemat-Nasser, S., 1983. Overall moduli of solids with microcracks: load-
326 induced anisotropy. J. Mech. Phys. Solids 31, 155–171.
- 327 Jasiuk, I., 1995. Cavities vis-a-vis rigid inclusions: elastic moduli of materials with
328 polygonal inclusions. Int. J. Solids Struct. 32, 407–422.
- 329 Jeffery, G.B., 1921. Plane stress and plane strain in bipolar co-ordinates. Philos. Trans.
330 R. Soc. Lond. Ser. A 221, 265–293.

- Kachanov, M., Sevostianov, I., 2018. Micromechanics of Materials, With Applications. Springer. 331
- Kachanov, M., Tsukrov, I., Shafiro, B., 1994. Effective moduli of solids with cavities 332 of various shapes. Appl. Mech. Rev. 47, S151–S174. 333
- Karunes, B., 1953. On the concentration of stress round the edge of a hole bounded 334 by two intersecting circles in a large plate. Indian J. Phys. 27, 208–212. 335
- Lanzoni, L., Radi, E., Sevostianov, I., 2018. Effect of cylindrical fibers of irregular 336 cross-section on the overall thermal conductivity of a composite. Int. J. Solids 337 Struct. 138, 264–276. 338
- Ling, C.-B., 1947. On the stresses in a notched plate under tension. J. Math. Phys. 26, 339 284–289. 340
- Ling, C.B., 1948a. On the stresses in a plate containing two circular holes. J. Appl. 341 Phys. 19, 77–82. 342
- Ling, C.B., 1948b. The stresses in a plate containing an overlapped circular hole. J. 343 Appl. Phys. 19, 405–411. 344
- Liu, X., Li, Y., Wang, J., He, Y., 2018. The pore growth process and pore coalescence 345 process in Gasar copper. Mater. Character. 137, 231–243. 346
- Radi, E., 2011. Path-independent integrals around two circular holes in an infinite 347 plate under biaxial loading conditions. Int. J. Eng. Sci. 49, 893–914. 348
- Sevostianov, I., Kachanov, M., 1999. Compliance tensors of ellipsoidal inclusions. Int. 349 J. Fract. 96, L3–L7. 350
- Shapovalov, V., 1994. Porous metals. MRS Bull. 19 (4), 24–28. 351
- Shapovlov, V.I., 1998. Formation of ordered gas-solid structures via solidification in 352 metal-hydrogen systems. Mater. Res. Soc. Symp. Proc. 521 (Symposium R), 281– 353 290. 354
- Shapovalov, V., Boyko, L., 2004. Gasar - anew class of porous materials. Adv. Eng. 355 Mater. 6, 407–410. 356
- Tsukrov, I., Novak, J., 2002. Effective elastic properties f solids with defects of irreg- 357 ular shape. Int. J. Solids Struct. 39, 1539–1555. 358
- Tsukrov, I., Novak, J., 2004. Effective elastic properties of solids with two- 359 dimensional inclusions of irregular shape. Int. J. Solids Struct. 41, 6905–6924. 360
- Zimmerman, R.W., 1986. Compressibility of two-dimensional cavities of various 361 shapes. J. Appl. Mech. 53, 500–504. 362
- 363